

In vivo three-dimensional spectral domain endoscopic optical coherence tomography using a microelectromechanical system mirror

Woonggyu Jung,¹ Daniel T. McCormick,² Yeh-Chan Ahn,¹ Ali Sepehr,¹ Matt Brenner,¹ Brian Wong,¹ Norman C. Tien,³ and Zhongping Chen^{1,*}

¹Beckman Laser Institute & Department of Biomedical Engineering, University of California, Irvine, USA

²Advanced MEMS, Berkeley, USA

³Department of Electrical and Computer Engineering, Case Western Reserve University, Cleveland, USA

*Corresponding author: z2chen@uci.edu

Received June 8, 2007; revised September 26, 2007; accepted September 26, 2007;
posted October 15, 2007 (Doc. ID 83969); published November 1, 2007

A biopsy is a well-known medical test used to evaluate tissue abnormality. Biopsy specimens are invasively taken from part of a lesion and visualized by microscope after chemical treatment. However, diagnosis by means of biopsy is not only variable due to depth and location of specimen but may also damage the specimen. In addition, only a limited number of specimens can be obtained, thus, the entire tissue morphology cannot be observed. We introduce a three-dimensional (3-D) endoscopic optical biopsy via optical coherence tomography employing a dual-axis microelectromechanical system scanning mirror. Since this technique provides high-resolution, noninvasive, direct, and multiple visualization of tissue, it could function as a clinical biopsy with advanced performance. The device was integrated with a conventional endoscope and utilized to generate *in vivo* 3-D clinical images in humans and animals. © 2007 Optical Society of America
OCIS codes: 170.0170, 170.2150, 170.4500.

Optical coherence tomography (OCT) is a minimally invasive imaging modality that permits high-resolution, cross-sectional imaging of scattering media in real time [1]. OCT has been proposed to have a potential role in “optical biopsy” [2,3] and subsequently applied to visualize numerous biological tissues. Because OCT has a limited penetration depth of 2–3 mm in scattering tissues, it usually requires the use of miniaturized optical beam delivery systems to image internal organs. To date, most endoscopic OCT applications have been focused on two-dimensional (2-D) imaging by linear [4] and/or rotational [5] scanning and require mechanical movement of the entire distal probe apparatus from the proximal end for scanning (usually through cable transduction methods). However, the capabilities of many mechanical probes are limited by cross talk, hysteresis, and 2-D constraints. For many clinical applications rapid 3-D imaging is highly desired to provide clinicians with fully realized diagnostic information, and reduced cross talk by elimination of movement of the imaging apparatus down the length of the probe is critical. During the past few years, the development of high-speed OCT systems such as spectral domain OCT (SD-OCT) had made real time 3-D OCT imaging possible [6,7]. Therefore, *in vivo* 3-D endoscopic imaging is now realizable and no longer limited by OCT system capabilities but by the development of high-speed advanced probes.

We report a 3-D endoscopic OCT system using a two-axis microelectromechanical system (MEMS) scanning mirror designed to realize this clinical need. Recently, the applications of MEMS scanning mirrors have been expanded from optical communication and sensors to optical imaging [8–10]. The reason for this widespread interest is due to the fact that MEMS technology has many advantages over prior designs,

including rapid scanning, small size, high reliability, and flexibility in scanning pattern capabilities. When this MEMS technology is applied to OCT systems, it allows miniaturization of bulky 2-D scanning probes without the functional drawbacks of other small OCT probes. Finally, it enables a method of acquiring 3-D images that provides the potential to deliver real time high-resolution diagnostic information to physicians as well as rapidly identify areas of interest during endoscopy.

Our OCT probe consists of a MEMS mirror and a pigtailed gradient index (GRIN) lens mounted in tubular steel housing (Figs. 1A and 1B). The MEMS scanning actuator is a monolithic, single crystal sili-

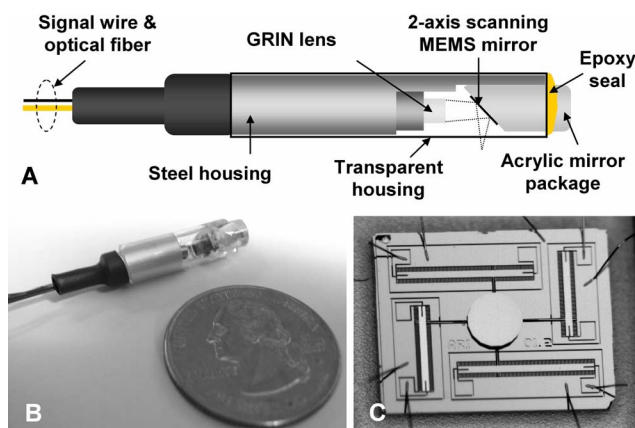


Fig. 1. (Color online) Developed MEMS-based OCT probe and scanning mirror: A, schematic of the 3-D endoscopic OCT probe. The steel lens housing contained a spacer to ensure proper working distance between the lens and mirror surface. B, completed probe compared for size with a U.S. quarter coin. The outer diameter of the probe was 5.5 mm. C, stereo microscope image of a two-axis MEMS mirror.

con, 2-D, gimbal-less, vertical comb-driven structure that exhibits x - and y -axis resonant frequencies of 1.8 and 2.4 kHz, respectively (Fig. 1C) [11]. When a voltage is applied to the vertical electrostatic comb-drive actuators, the mirror is scanned about the torsion springs in both axes. The scan angle of each axis was approximately 20° (optical). This probe used steel tubes to provide rigidity and alignment of the GRIN lens to the MEMS mirror. The total length of probe was 2 m with a 2 cm rigid portion at the distal end. The specific GRIN lens ($\phi 1.4$ mm) utilized in this study had a 6.6 mm working distance.

The MEMS-based OCT probes were integrated with conventional endoscopes including a flexible fiber-optic bronchoscope and rigid rod-lens telescope. Figures 2A and 2C show how the probe is tethered to the endoscope. The probe was oriented so that the OCT beam scanned across the endoscope field of view. The integrated light source of the flexible and rigid endoscopes coupled with cameras was used to guide the path of the OCT probe. Hence, the axial and rotational orientation and positioning of the OCT probe relative to the target tissue were determined by direct endoscopic visualization. Figures 2B and 2D show the image captured by the endoscope camera, which identified the location and guided the positioning of the OCT probe in the airway. In our experiment, the endoscopic light source was adjusted to 10–25% of maximum illumination to allow concurrent visualization of the guide beam from the OCT probe (dotted line in Fig. 2D). Finally, OCT probes combined with endoscopes were incorporated with the sampling arm of a fiber-based SD-OCT system [10].

In the SD-OCT system, a low-coherence light having a center wavelength of 1310 nm with a full width at half-maximum bandwidth of 95 nm was coupled into a fiber-based Michelson interferometer. Backreflected light from the reference and sample arms was guided into a spectrometer. The dispersed spectrum was sampled by a 1×1024 InGaAs detector array at 7.7 kHz. The wavelength range on the array was 130 nm, corresponding to a spectral resolution of 0.13 nm. When the optical paths at both arms matched, an interference pattern was generated on the detector array. A 2-D image was generated by acquiring a depth-modulated signal sequentially while the fast axis of the MEMS mirror scanned. Then, the slow axis of the MEMS mirror moved to the next position and 2-D images were reconstructed to form the 3-D images. The lateral and axial resolutions of the reconstructed image are determined by the beam waist at the focal point and the coherence length of the source; these resolutions were 20 and 10 μm , respectively.

Rabbit and human tissues were imaged *in vivo* (Fig. 3) with the integrated 3-D endoscopic OCT probe employing an SD-OCT system (8 frames/s), which was adequate to eliminate artifacts seen at slower scan rates. *In vivo* 3-D OCT images of rabbit rectum and corresponding histology are shown in Figs. 3A and 3B, respectively. These images were obtained with the OCT probe guided by bronchoscope. The OCT images correlated very closely with conven-

tional histologic sections, and the tissue layers (mucosa, muscularis mucosa, submucosa, and muscularis propria) were readily identified. Figure 3C demonstrates a 3-D OCT image of human finger that provides clear visualization of tissue structures, such as the epithelial layer, epidermal layer, and sweat ducts. This image demonstrates one major advantage of 3-D over 2-D imaging, as the spiral morphology of the sweat duct can only be directly visualized with the former. In similar fashion, 3-D images may more robustly identify the borders and margins of lesions such as early microinvasive cancers. The OCT probe coupled to a rigid endoscope was used to image the upper airway of human patients during surgical endoscopy. For optical imaging, a suspension laryngoscope was inserted and fixed in place under general anesthesia. OCT images were obtained under direct endoscopic visualization. 3-D OCT images of the epiglottis and true and false vocal cords were obtained. A representative image of the true vocal cord clearly shows the stratified squamous epithelium, basement membrane, and superficial lamina propria (Fig. 3D).

Considering these results, we have identified two major potential advantages of rapid 3-D high-resolution endoscopic OCT as a biopsy function compared with conventional excisional or image guided biopsy. First, the boundaries of lesions can be better defined using arrayed 3-D optical sectioning. Since OCT has micrometer-scale resolution, ranging from 2 to 20 μm , it not only gives resolution comparable with that of excisional biopsy but also better delineates the boundaries of complex structures and lesions than image guided biopsy. 3-D imaging obtains volumetric data on tissue structure and can be reformatted to allow analysis of 2-D sections in any user-defined image plane. Using surface rendering and segmentation algorithms, complex 3-D reconstructions of microvascular or other tissue/organ substructures can be obtained at micrometer-level resolution.

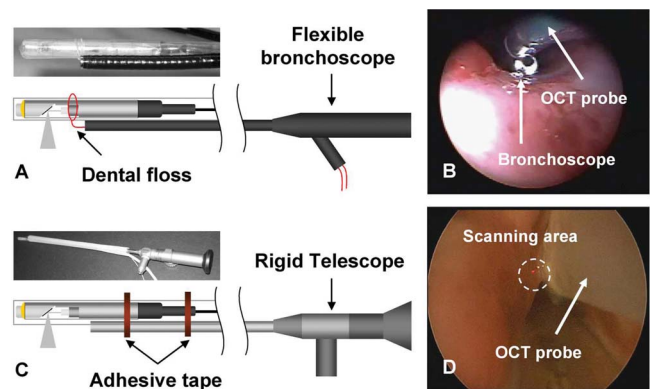


Fig. 2. (Color online) OCT probe incorporated with endoscopes: A, schematic and photograph of the OCT probe assembly with the flexible bronchoscope. By string loop methodology using dental floss, the OCT probe was affixed to the bronchoscope. B, image of OCT probe tethered to the flexible fiber-optic bronchoscope in pig trachea. C, schematic and photograph of the OCT probe incorporated with the rigid telescope. D, a rigid endoscope camera guides the location and movement of the OCT probe in the human airway for visualization and directed passage through upper airways.

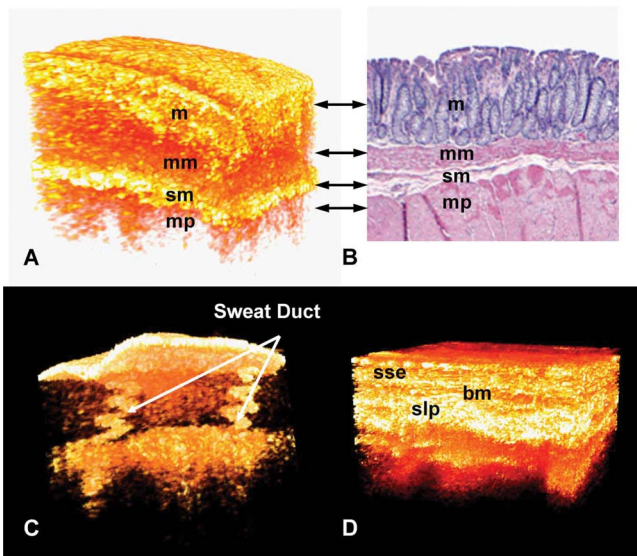


Fig. 3. (Color online) *In vivo* 3-D OCT images obtained by the SD-OCT system. An imaging volume of $1\text{ mm} \times 1\text{ mm} \times 1.4\text{ mm}$ with $10\text{ }\mu\text{m}$ voxels was acquired within 15 s. A, B, *In vivo* OCT images and histology of a rabbit rectum. The 3-D OCT image correlated very well with histology: mucosa (m), muscularis mucosa (mm), submucosa (sm), and muscularis propria (mp). C, *In vivo* images of a human finger; the arrows indicate the sweat ducts which are visualized as spiral shaped. D, True human vocal cord: important structures such as the stratified squamous epithelium (sse), basement membra (bm), and superficial lamina propria (slp) are clearly visible.

These functional features may have potential applications in cancer detection, assessment of injury and remodeling, and quantitative assessment of response to therapy with capabilities for regional response differentiation. One drawback of excisional biopsy is structural damage to tissue, which limits sampling of tissues in critical regions such as the vocal cords and retina. We illustrated an example of vocal cord imaging (Fig. 3D) because the vocal cords lose functionality with biopsy. Biopsy of the vocal cords leads to scarring that leads to an alteration in the vibratory patterns during phonation, leading to a change in voice quality. With high-resolution 3-D image guidance, biopsies could be directed to regions of higher diagnostic yield, and tumor resection margins could be better defined and thus more precisely excised. In addition, there are number of disease areas where rapid high-resolution 3-D optical biopsy has obvious clinical applications, such as aerodigestive tract cancer detection, inflammatory bowel disease, arthros, pulmonary inhalation injury [12], and other cancer detections [13], to name just a few.

In summary, a 3-D endoscopic OCT device based on MEMS technology was designed, constructed, and integrated with conventional endoscopes. The OCT probe was positioned and maneuvered using an endoscope in human and animal studies. Rapidly acquired 3-D images of living tissue visualized detail structures that were comparable with those of standard

histology. With the current device, we secured the probe to the outside of endoscopes due to the size of the MEMS mirror and actuator. However, further reduction in the MEMS probe profile and diameter could allow placement within the working channel of a standard endoscope. Since this technique provides high-resolution, noninvasive, direct imaging of tissue anatomy, it may be valuable in directing biopsies toward regions of high diagnostic yield, directing therapy, and also monitoring the progression of disease.

The authors acknowledge the contribution of V. Milanović at the Adriatic Research Institute for mirror fabrication and David S. Mukai for help with animal preparation, regulatory compliance, and sample processing. We also thank William B. Armstrong, for providing volunteer patients from whom to obtain images of the human upper aerodigestive tract. Advanced MEMS is also gratefully acknowledged for providing the probe and control system. This work was supported by research grants from the National Science Foundation (BES-86924), National Institutes of Health (EB-00255, NCI-91717, RR-01192), the Air Force Office of Scientific Research (FA9550-04-1-0101), and the Beckman Laser Institute Endowment.

References

1. D. Huang, E. A. Swanson, C. P. Lin, J. S. Schuman, W. G. Stinson, W. Chang, M. R. Hee, T. Flotte, K. Gregory, and C. A. Puliafito, *Science* **254**, 1178 (1991).
2. J. G. Fujimoto, M. E. Brezinski, G. J. Tearney, S. A. Boppart, B. Bouma, M. R. Hee, J. F. Southern, and E. A. Swanson, *Nat. Med.* **1**, 970 (1995).
3. W. B. Armstrong, J. M. Ridgway, D. E. Vokes, S. Guo, J. Perez, R. P. Jackson, M. Gu, J. Su, R. L. Crumley, T. Y. Shibuya, U. Mahmood, Z. Chen, and B. J. Wong, *Laryngoscope* **116**, 1107 (2006).
4. B. E. Bouma and G. J. Tearney, *Opt. Lett.* **24**, 531 (1999).
5. G. J. Tearney, M. E. Brezinski, B. E. Bouma, S. A. Boppart, C. Pitris, J. F. Southern, and J. G. Fujimoto, *Science* **276**, 2037 (1997).
6. S. Yun, G. Tearney, B. Bouma, B. Park, and J. de Boer, *Opt. Express* **11**, 3598 (2003).
7. Y. Ahn, W. Jung, J. Zhang, and Z. Chen, *Opt. Express* **13**, 8164 (2005).
8. W. Jung, D. T. McCormick, J. Zhang, L. Wang, N. C. Tien, and Z. Chen, *Appl. Phys. Lett.* **88**, 163901 (2006).
9. W. Piyawattanametha, R. P. J. Barretto, T. H. Ko, B. A. Flusberg, E. D. Cocker, H. Ra, D. Lee, O. Solgaard, and M. J. Schnitzer, *Opt. Lett.* **31**, 2028 (2006).
10. J. T. C. Liu, M. J. Mandella, H. Ra, L. K. Wong, O. Solgaard, G. S. Kino, W. Piyawattanametha, C. H. Contag, and T. D. Wang, *Opt. Lett.* **32**, 256 (2007).
11. V. Milanović, G. A. Matus, and D. T. McCormick, *IEEE J. Sel. Top. Quantum Electron.* **10**, 462 (2004).
12. W. Jung, J. Zhang, R. M. Araghi, N. Hanna, M. Brenner, J. S. Nelson, and Z. Chen, *Lasers Surg. Med.* **35**, 121 (2004).
13. W. Jung, J. Zhang, J. Chung, P. W. Smith, M. Brenner, J. S. Nelson, and Z. Chen, *IEEE J. Sel. Top. Quantum Electron.* **11**, 811 (2005).